13 Aug 2008, 9:45 am - 10:30 am

Evaluation of the Experiences in Underwater Dam Construction on Soft Soils

W. F. Van Impe

Ghent University, Ghent, Belgium

6th International Conference on
Case Histories in Geotechnical Engineering, Arlington, VA, August 11-16, 2008

EVALUATION OF THE EXPERIENCES IN UNDERWATER DAM CONSTRUCTION ON SOFT SOILS

W.F. VAN IMPE
Ghent University, Laboratory of Soil Mechanics
9052 Zwijnaarde, Ghent, Belgium

ABSTRACT

The present paper illustrates the outcome of the monitoring of the consolidation behavior of a soft foundation soil under a large submerged sand embankment. Measurements of settlements and excess pore water pressures showed a good agreement with predictions evaluated using the large strain consolidation theory. Soft soil improvement by means of deep mixing has been optimized. Moreover, the principles and developments of underwater geosynthetics applications are discussed.

INTRODUCTION

As in many harbor areas all around the world, the harbor of Antwerp is experiencing an increasing need of storing capacity for excavated soil or dredged material from construction projects and maintenance of waterways. Such need has encouraged the design and currently ongoing construction of a partially submerged embankment, with an approximate height of 27 m, sub-dividing an existing dock (Doel) and using the available dock space behind the embankment to store the dredged material (Figure 1). The challenge of this project was the fact that the embankment had to be built on a very soft soil deposit (not removable because of geoenvironmental considerations) of sedimentations under own weight consolidation.

Figure 1 illustrates the final design choice out of an optimization in which numerous preliminar design options were worked out. Given the soft consistency and very low bearing capacity of the foundation soil, it became clear that some kind of foundation layer reinforcement was required. Therefore ground improvement by a novel deep mixing technology, SSI (Soft Soil Improvement), was proposed. A detailed description of this technology and properties of the treated soil is reported in detail by Van Impe & Verastegui (2006).

As illustrated in the figure 1, only the foundation soil at the toes of the embankment was improved by installing SSI deep mixing columns. These improved zones were meant not only to provide extra safety but also to confine the inner part of the soft soil layer under the embankment.

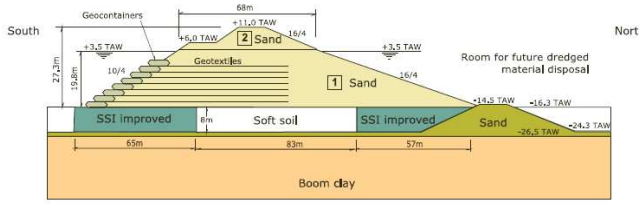

Figure 1. Scheme of the partially submerged embankment design

A slope stability analysis showed, as expected, that short-term stability (that is the construction phase) was the most critical. So, special measures had to be taken to avoid early instability problems. Unavoidably, a staged construction was implemented. Since staged construction relies on the strength increase of a foundation soil due to ongoing consolidation, an accurate evaluation of the consolidation degree had to be achieved.

However, initial estimations of consolidation degree (at the design stage) showed a considerable difference between the consolidation behavior of the soft soil when implementing small strain consolidation theories (e.g. Terzaghi) and large strain consolidation (e.g. Gibson et al., 1967).

SOIL PROPERTIES

The foundation soil of the embankment consists of a 8m layer of soft dredged material overlying a thin layer of sand and a deep layer of Tertiary Boom clay (highly overconsolidated). The foundation soil is located under water at a depth of about 19m. The soft soil studied here is a soft deposit of fine grained material, result of a prolonged sedimentation and self-weight consolidation process of dregs removed from waterways within the harbor of Antwerp. The consistency of the soil remained quite soft even after attempts of accelerating its consolidation by means of vacuum. The natural water content of the soil was of the order of 115%, the plasticity index of the order of 77 and the organic content of about 6%. Table 1 summarizes more approximate physical properties of this soil.

The initial in-situ undrained shear strength (c_u) of this deposit of soft dredged material was estimated by means of extensive laboratory and field testing. In general, the average c_u ranges from about 2 to 4 kPa and it was observed to increase linearly with depth, suggesting that the deposit is mainly in a normally consolidated state.

The consolidation behavior of the soft dredged material was assessed by means of Constant Rate of Strain (CRS) tests, hydraulic conductivity tests and oedometer tests. Figure 2 summarizes the results of all tests performed. Out of a fitting procedure, two constitutive equations relating hydraulic conductivity (k), void ratio (e) and effective stress (σ'_v) could be obtained (Eq. 1 & 2).

Table 1. Physical properties of the soft soil

Index	Value
Liquid limit (%)	124.4
Plastic limit (%)	46.7
Natural water content (%)	115.0
Organic matter (%)	6.0
Carbonate content (%)	13.9
Sand (%)	10.4
Wet density (g/cm³)	1.3-1.4
pH of pore water	7.2

$$k = 6 \cdot 10^{-8} \cdot \sigma'^{-1.18}_{v} \text{ (m/sec)} \qquad (1)$$

$$k = 6 \cdot 10^{-12} \cdot e^{5.52} \text{ (m/sec)} \qquad (2)$$

Although with some scatter (more pronounced in the high void ratio zone), both equations attempt to describe the consolidation behavior of the soil for the full range of void ratio, starting from the freshly sedimented situation.

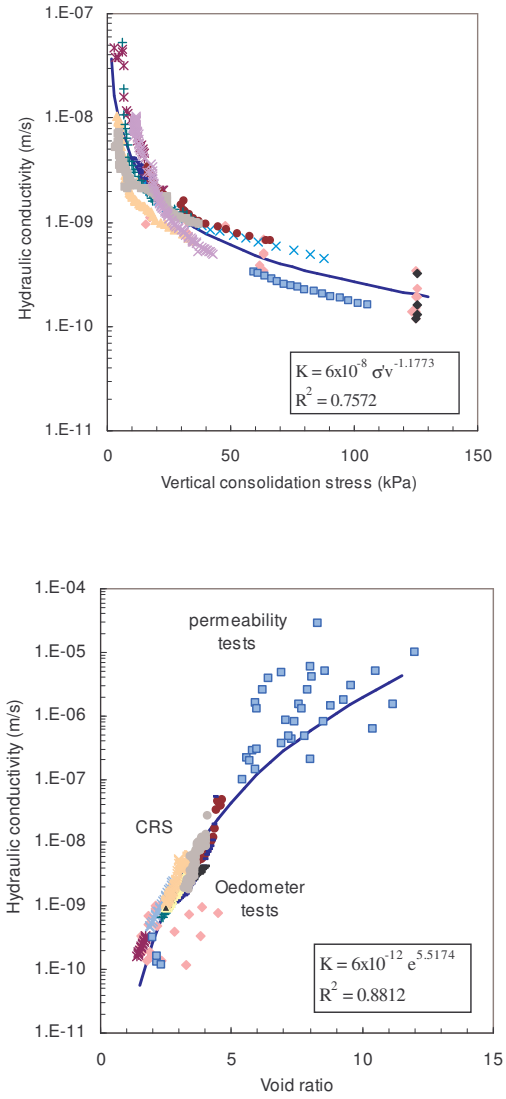

Figure 2. Consolidation properties of the soft soil

IMPROVEMENT OF THE FOUNDATION SOIL

The foundation soil (at the toes of the embankment) was improved by implementing a novel deep mixing technique, the SSI (soft soil improvement). The SSI technique could be classified as a wet deep mixing technique as it injects cement slurry. Moreover, it makes use of pressurized mixing by means of a mixing tool provided with 2 sets of nozzles distributed all along the full diameter of the column (Fig. 3).

The mixing tool is fixed to a main drilling rod and each set of nozzles is connected to independent injection systems. A high-pressure injection system (of the order of 20 to 30 MPa) cuts the soil and allows for intense mixing while the low pressure injection system (up to 5 MPa) just adds the remaining amount of cement slurry to fulfil the required dosage.

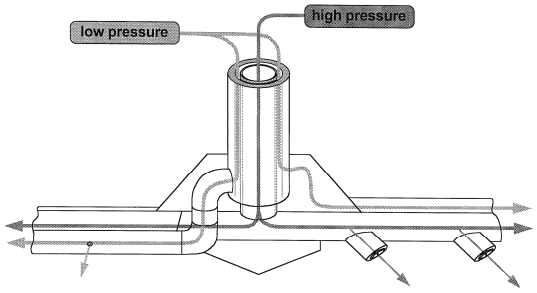

Figure 3. SSI mixing tool

A quite important issue in the design of deep mixing columns is the choice of cement. In order to do that an extensive laboratory research was carried out aiming at evaluating the improvement level of mixes with e.g. Portland cements (binders D), Blast furnace cements and others (Van Impe & Verástegui, 2006). Out of that research, blast furnace cements (binders B) were chosen as the most suitable for the improvement of the soft sludge (Fig. 4a). In fact, portland cements were observed to quickly improve the soil during the first month only. On the other hand, blast furnace cement showed a slow but continuous improvement that did not end even after about 2 years reaching in the end a higher strength than Portland cements. Blast furnace cements (binders B)are also known to have a better performance in marine environments.

The chosen cement type was transformed into a slurry (w/c ratio = 0.8) and injected during downwards and upwards operation of the drilling rod to accomplish a binder dosage of about 275 kg/m^3 approximately.The actual level of improvement in the site was checked by testing of core specimens in the laboratory. The cores were sampled 56 days after installation of the SSI columns. Figure 4b illustrates the results of unconfined compression tests. The unconfined compressive strength in the dredged material layer ranged from 1 to 5 MPa. Not only the design strength was (by far) exceeded, but also the strength out of laboratory tests which showed the good performance of the implemented improvement technique.

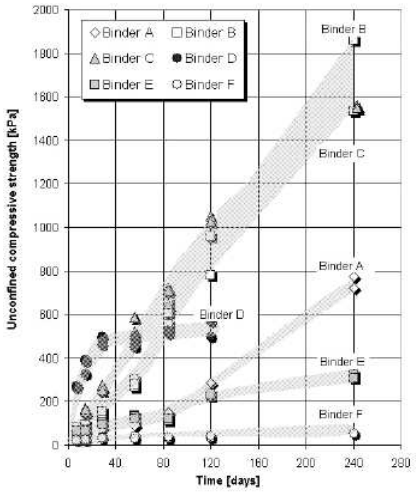

Figure 4a. UC strength of specimens (T = 10°C)

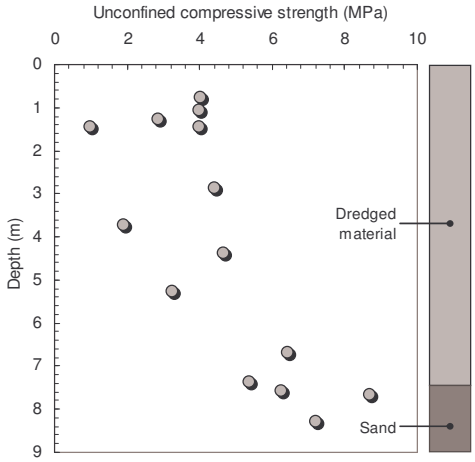

Figure 4b. Unconfined compressive strength of SSI column core specimens (56 days after installation)

The most commonly used cement types for stabilization are Portland cement and Blast furnace cement. Portland cements are inorganic binders obtained by grinding to a high fineness, Portland clinker alone, or most commonly in combination with calcium sulfate (gypsum) acting as a set regulator. In ordinary Portland clinker, tricalcium silicate (C_3S) is the most abundant phase present in amounts between about 50% and 70%. Dicalcium silicate (C_2S) usually constitutes 15-30% of the clinker. Typical amounts of tricalcium aluminate (C_3A) are 5-10% and of the ferrite phase (C_4AF) 5-15%. During the hydration of the cement a C-S-H phase is formed and $Ca(OH)_2$ is released. The first hydration product has high strength which increases as it ages, while $Ca(OH)_2$ contributes to the pozzolanic reaction as in the case of lime stabilisation.

Figure 5 illustrates the cement stabilization mechanism. Immediately after mixing it is possible to identify clay clusters and cement paste as separate phases. Next, the strength of the stabilized soil will gradually increase due to pozzolanic reactions within the clay clusters and hardening of the cement paste.

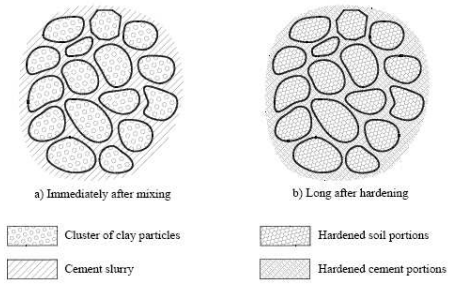

Figure 5. Cement stabilization mechanism (CDIT, 2002)

Blast furnace cement is a mix of Portland cement and blast furnace slag and shows a similar stabilization mechanism. Finely powdered slag does not react with water but it has the potential to produce pozzolanic reaction products under high alkaline conditions. The SiO_2 and Al_2O_3 contained in the slag are actively released by the stimulus of the large quantities of Ca^{2+} and $SO^{2/4}$ from the cement, so that a hydration product is formed for which the long-term strength is enhanced. The complicated mechanism of stabilization has been simplified by Saitoh et al. (1980) in Figure 6 for the chemical reactions between clay, pore water, cement and slag.

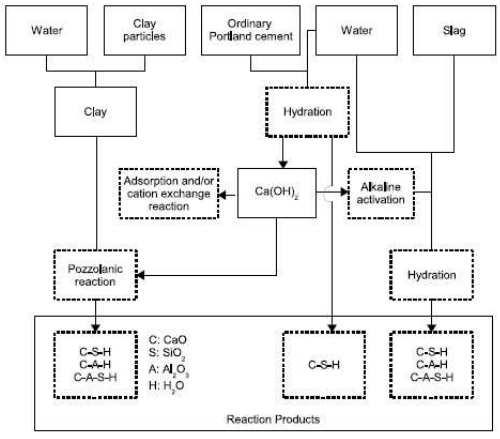

Figure 6. Chemical reaction among clay, cement, slag and water (Saitoh et al., 1985)

The soil collected from the soft deposit was thoroughly homogenised and remolded prior to mixing with cementing agents. A dough mixer was employed here to mix the soil and a slurry of cement.

The dosage of binder for mixing with soil was set to 275 kg/m^3, the water/cement ratio of the slurry was set to 0.8 and a mixing time of about 10 minutes was implemented. This extended mixing time was meant to allow for more intensive mixing; however, only a slight difference in strength was observed when compared to specimens mixed for 5 minutes (less than 5% after 7 days). Cylindrical specimen with a diameter of 57 mm and a height of 115 mm were prepared by pouring the mix into split plastic moulds. The moulds were later sealed with paraffin film and stored under water in a conditioned room at 10 C with no overburden whatsoever acting on the specimen. In addition, some specimen were cured under water at 20° C in order to study the effect of the temperature on the development of the improvement.

At the initial stage of this project, a number of different types of cement have been employed in the laboratory. A short description (according to EN 197-1) of the binders is given below:

* Binder A, B, and C are all blast furnace cements, CEM III. Binder C has the greatest blast furnace slag content (CEM III/B). Binder B and C classify at a nominal strength of 42.5 MPa while binder A has only 32.5 MPa.
* Binder D is a Portland cement, CEM I, with a nominal strength of 52.5 MPa.
* Binder E is a commercially available binder specifically designed for stabilization of soil.
* Binder F is a cement typically used for soil grouting purposes.

A large number of unconfined compression tests have been performed at several time intervals (i.e. 7, 14, 28, 56, 84, 120, 240 and 550 days). The results of the testing programme on specimen cured under water at 10 C have already been reported by Van Impe et al. (2004b) and are summarized in Figure 7.

From the group of binders tested here, it seems that the blast furnace cements (binders A, B and C) perform quite well, showing a continuous increase of the UC strength. Binders B and C (both CEM III 42.5) do show an unconfined compressive strength of the order of UCS 2.2 MPa after 550 days. The Portland cement (binder D), on the other hand, allows for more rapid hardening in the first days. In fact, it shows the highest UC strength during the first month. However, the improvement provided by Portland cement seems to decline afterwards for some period to finally pick up again after some 3 months. The understanding of why systematically this ”interval” of the interplay cement-soil occurs is subject to further research today. Anyhow, the final compressive strength of Portland cement remains lower than that given by the blast furnace cements B and C. The other binders (E and F) seem to produce little improvement for such high dosage (UCS 0.7 MPa after 550 days).

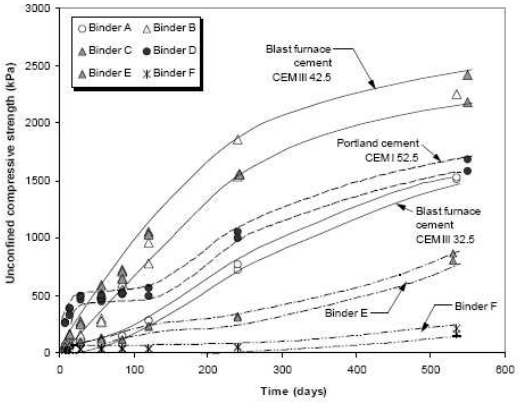

Figure 7. UCS of cement stabilised specimen cured underwater at 10°C

The strain at failure of specimen cured under water at 10° C, illustrated in Figure 8, was measured externally (from top to bottom cap of a triaxial cell) by LVDT. The figure provides some information about the ductility of the stabilised mass.

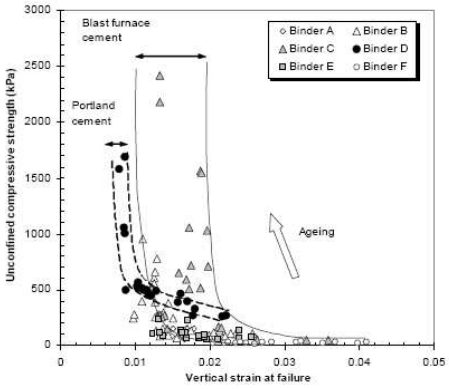

Figure 8. Strain at failure of cement stabilized specimen cured under water at 10°C

In spite of some scatter it seems possible to establish a general tendency of behaviour for each binder mix. Overall, the strain at failure (ranging from 0.9% to 4%) decrease rapidly with increasing UC strength. The brittleness increases obviously with increasing UCS values. From the results it can also be deduced that, as ageing increases, specimen mixed with Portland cement tend to yield at smaller axial strains than specimen mixed with blast furnace cement, even tough the strength of specimen mixed with Portland cement is considerably lower. Measurements of small-strain modulus were also performed by means of bender element testing at different time intervals for some specimen (cured under water at 10° C) mixed with blast furnace cement (Binder C) and with Portland cement (Binder D) only.

The bender element test set up employed here is given in Figure 9. The principle of this non-destructive method is simple and well know from literature (Dyvik & Madshus, 1985). As an example, Figure 10 illustrates the S-wave arrival time measured for specimen stabilised with blast furnace cement at several curing time intervals using an input sinusoidal pulse with a frequency of 4 kHz. Each specimen was tested for unconfined compression to measure UCS. As expected, a rather linear relationship between G_0, E_0 and UCS is observed.

Figure 11 summarizes the Young's modulus at small strain E_0 evaluated here for specimen mixed with Portland and blast furnace cement. The modulus for the Portland cement was found to be slightly higher but still, a single linear correlation has been proposed for both cements: $E_0 \approx 714$ (UCS).

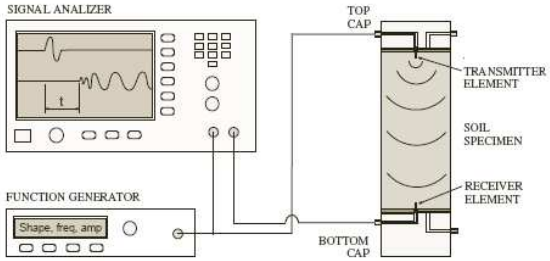

Figure 9. Bender elements testing setup

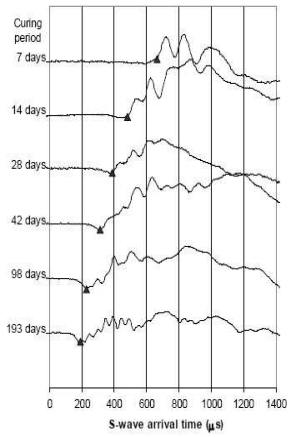

Figure 10. Shear wave arrival time measured at several curing time intervals on specimen mixed with blast furnace cement and cured under water at 10°C

Similarly, Figure 11 illustrates the secant Young's modulus evaluated from unconfined compression tests. Even if trend shows some scatter, the data could be more or less linearly correlated to UCS as well. It has been estimated as $E_{S50} \approx 110$ (UCS) . This trend is considerably low when compared to the Japanese experiences reported by Saitoh et al. (1980) where 350 (UCS) < E_S50 < 1000 (UCS) ; however, it falls within the range of many other correlations proposed worldwide in the

literature (Porbaha et al., 2000). Overall, the modulus of the Portland cement is slightly higher than that given by the blast furnace cement. In general, E_0 remains about 7 times E_{S50} .

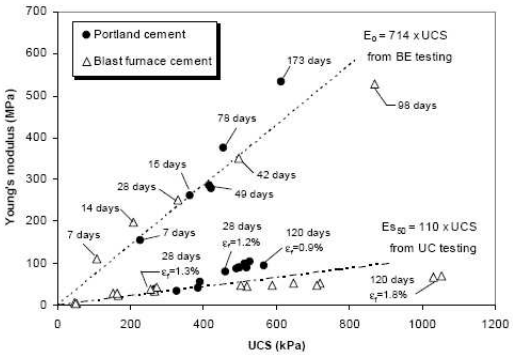

Figure 11. Young's modulus at small strain levels (E_0) and secant Young's modulus at 50 % of deviatoric stress (E_{S50}) versus UCS

In an attempt to more reliably recreate the conditions in the field, a large cylindrical specimen with a height H ≈ 0.8 m and diameter ∅ ≈ 0.6 m was prepared in the laboratory employing blast furnace cement, with the aim of evaluating and monitoring the temperature changes due to exothermic reactions within the stabilized mass. The virgin soil was kept at a temperature of 10° C prior to mixing. After mixing of the soil and blast furnace cement slurry in a concrete mixer, the stabilized mass was poured into a large plastic mold (also stored at 10° C and with the above mentioned dimensions) where eight temperature transducers (labeled T1, T2...T8) were installed at different locations within the sample.A few small cylindrical specimen were also prepared and cured (under water at 10° C) following the ordinary procedure described in a previous subsection.

The temperature measurements within the stabilized mass over a period of 56 days are illustrated in Figure 12.

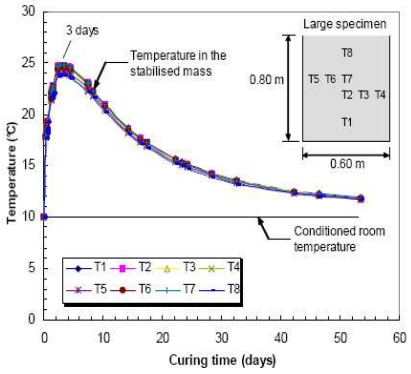

Figure 12. Hydration temperature monitoring on large specimen mixed with blast furnace cement and stored in a conditions romm at 10°C

The readings of all temperature transducers do show a common trend. Immediately after mixing a sudden temperature increase was observed. After 3 days a maximum temperature of about 25° C was reached. Finally, the temperature in the large specimen seems to gradually decrease; after 56 days, the temperature (about 11.7° C) leveled out at values only slightly over the conditioned room temperature (10° C).

By the end of the temperature monitoring some core samples were taken from the large specimen. Figure 13 shows the UCS of such core samples.

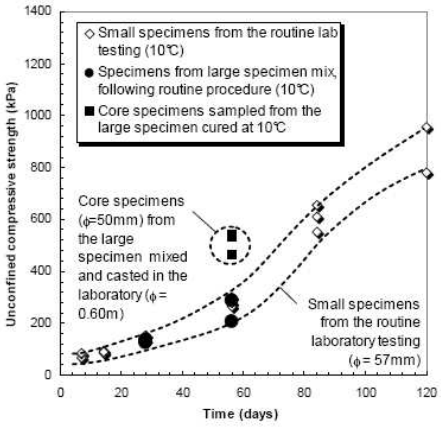

Figure 13. UCS of core specimen from a large stabilized specimen

The figure also indicates the UCS of small specimen from the routine laboratory testing as described in a previous subsection. Clearly, the UCS of the large specimen cores doubles the UCS values of the small specimen. This suggested that the transient temperature increase due to the exothermic reactions within the large specimen were imposing such notable difference. Indeed, the larger the sample, the slower the heat dissipation and so the higher the UCS to be expected.

In order to study the effects of the curing temperature on the UC strength of the stabilized dredged material an extra series of tests has been carried out; this time on small specimen mixed with blast furnace cement, cured under water at 20° C. The results (Figure 14) demonstrated that the strength of the samples stabilized with blast furnace cement is notoriously affected by the temperature. The hydration of the blast furnace cement clearly benefits from high temperatures; in fact, the UCS of samples cured under water (up to 200 days) at 20° C is, at all times, about 1.7 to 2 times larger than the UCS of specimen cured at 10° C.

The experimentation for the evaluation of properties of the cemented soil in the field consisted of core sampling of specimen from trial columns to proceed later on with unconfined compression tests in the laboratory.

The trial deep mixing columns (∅ ≈ 1.9 m) were installed in the site (underwater) with the SSI technique from a jack-up platform. Only blast furnace cement (Binder C) was used for the field experimentation. The cement was mixed with water an transformed into a slurry (w/c =0.8) on land. The cement slurry was pumped to the jack-up platform by means of floating pipes. In order to optimize the column installation rates the jack-up platform was provided with a moon pool to allow the installation of 22 to 24 columns in each zone covered by the platform. State of the art positioning systems ensured a very precise location of each column.

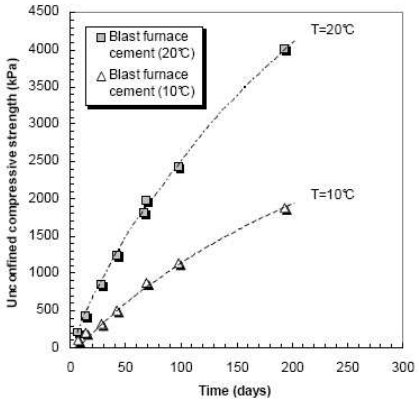

Figure 14. Effect of the curing temperature on the UCS of specimen mixed with blast furnace cement

The optimising of the SSI cement binder type was done following a research programme on hundreds of samples. In order to evaluate the improvement of the dredged material, untreated specimen, laboratory reconstituted and mechanically mixed cement-stabilised specimen and undisturbed sample from borings in the SSI cementstabilised columns (implementing binder C, a blast furnace cement), have been analysed by means of Scanning Electron Microscopy (SEM) aiming at investigation of the microstructure and composition of each specimen.

Specimen of untreated dredged material have been analysed on SEM. The specimen were prepared to simulate the natural in situ conditions of the dredged material with light compaction and it were carefully dried prior to the test. Figures 15 and 16 do illustrate SEM pictures with amplifying factors of 500 and 1100 respectively. Clay particles (platy shaped) can be identified by their more bright colour in the pictures. They seem to be uniformly spread and are interacting with the silt and sand particles (in edgy or rounded shape and darker in colour). It is also possible to find traces of organic material showing a very regular micromorphology.

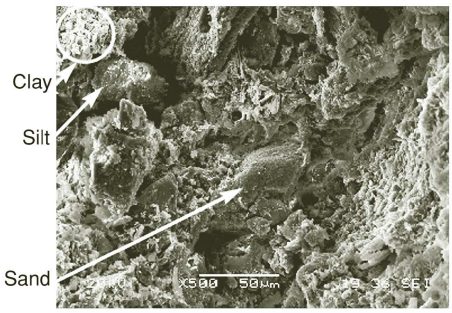

Figure 15. Untreated dredged material specimen - amplification factor x 500

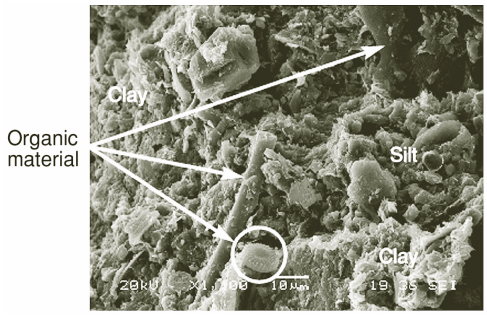

Figure 16. Untreated dredged material specimen - amplification factor x 1100

Figures 17 and 18 do show the specimen (4 cm × 4 cm × 1 cm) carefully cut with a water-cooled sawing system, starting from stabilised samples either mixed in the laboratory either from SSI field samples. It is clear already from this pictures that the specimen differ in texture. At the moment of the microscopy analysis, the sample from the laboratory was for example about 300 days old and had been kept sealed, under water, in a T =10 °C conditioned room.

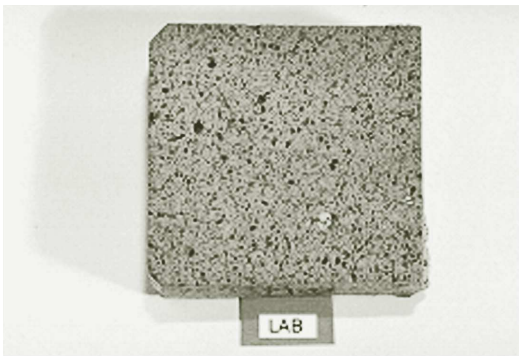

Figure 17. Mechanically cement-stabilized specimen prepared in the laboratory

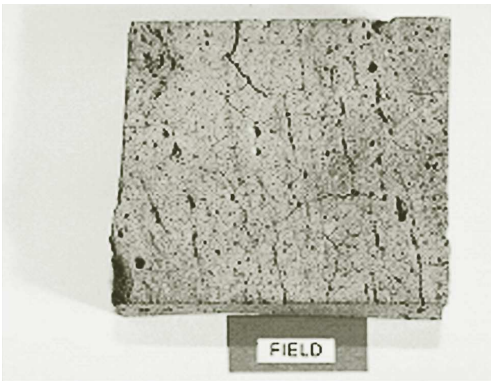

Figure 18. SSI cement-stabilized specimen from field boring

On the other hand the sample from the field as well was about 270 days old; this specimen was cored from a trial SSI column about 3 months after its installation and then it was kept under water as well, until the day of SEM analysis. Figures 19 and 20 do show both specimen with an amplification factor of 35. The presence of large pores (>5¡ m in diameter) and macro pores (>0.05¡ m in diameter) in the laboratory specimen is evident. This is by far less pronounced in the SSI improved field specimen where a more compact and more homogeneous texture can be seen.

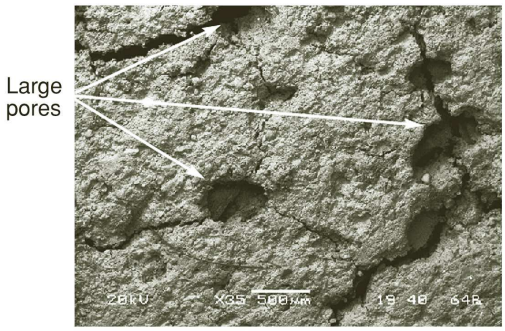

Figure 19. Laboratory specimen - amplification factor x 35

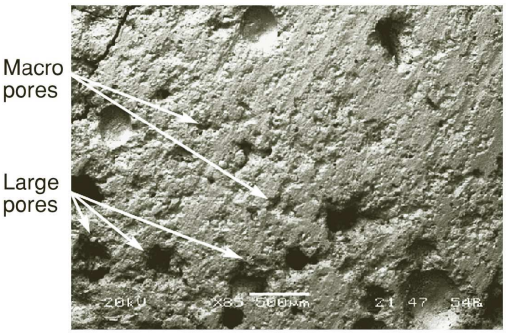

Figure 20. SSI-improved field specimen - amplification factor x 35

At this point one might already state that the mechanical cement-mixing in the laboratory (by means of a dough mixer) could have caused the incorporation of air bubbles later becoming large pores.

Pores of smaller diameter (micro pores) observed in both specimen could have produced during the cement hydration process. The presence of macro pores in the laboratory prepared samples suggests already a lower strength in the specimen mixed in the laboratory. Figures 21 and 22 do illustrate the specimen from the laboratory and the SSI-improved field sample, this time with an amplification factor of 1200. It is, again, quite clear that the micro structure is diverse. The specimen from the field has a much more homogeneous structure with a more regular disposition of hydration products, such as the calcium silicate hydrate (C-S-H phase) and the calcium hydroxide (CH). On the other hand, the mechanically mixed laboratory samples show a rather heterogeneous composition. Judging for the morphology of the different C-S-H phase structures and the large CH crystals, clearly identified, a less advanced degree of hydration can be perceived in the laboratory samples.

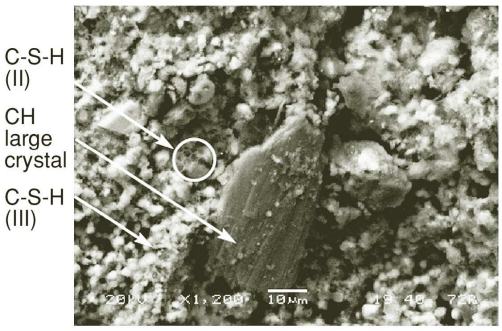

Figure 21. Laboratory specimen - amplification factor x 1200

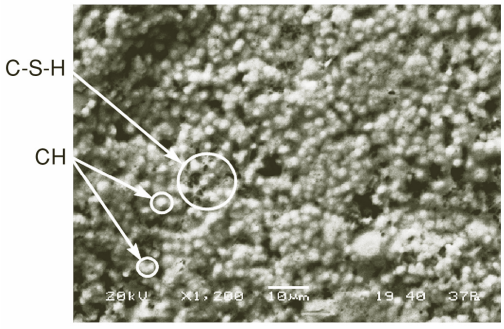

Figure 22. SSI-improved field specimen - amplification factor x 1200

Here one may also suggest that the much more intensive SSI mixing method has played an important role (the specific area around each soil particle has been reached by the binder, by far better). It seems that the highpressure SSI mixing in the field has improved the distribution of cement particles around the soil particles and as a consequence a faster hydration and hardening has taken place. In the laboratory, where purely mechanical mixing with a dough mixer was put into practice, the cement paste may have not been well distributed only reaching the soil particles within clods. This causes a retardation in the overall hardening of the improved mass and a decrease in the final strength.

Finally, figures 23 and 24 do illustrate the sample mixed in the laboratory and the SSI improved field sample with an amplification factor of 1700. Also here one can observe the same pattern, the structure of the field specimen again looks much more homogeneous than the laboratory specimen. In the pictures one can clearly identify the main hydration products of the cement (ODLER 2000). The (mature) C-S-H phase can be recognized in the field specimen together with uniformly distributed CH crystals that cover almost completely the soil.

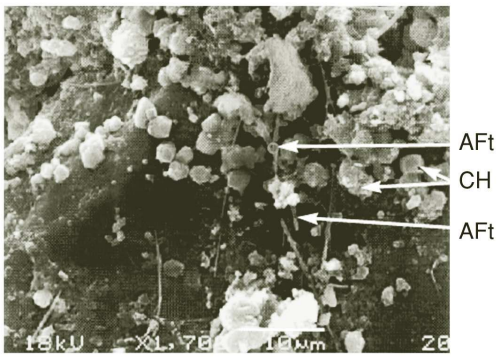

Figure 23. Laboratory specimen - amplification factor x 1700

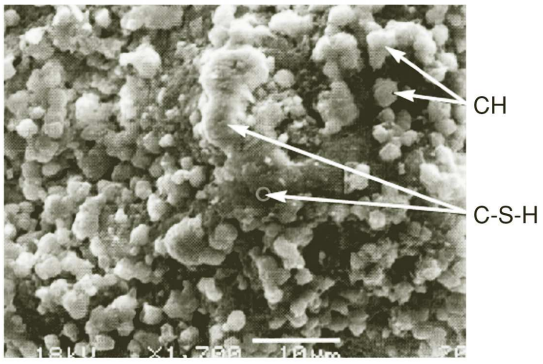

Figure 24. SSI-improved field specimen - amplification factor x 1700

As expected, again, the laboratory sample shows less CH crystals, few and small portions of the C-S-H phase and some ettringite (AFt phase) that is formed during the early hydration process, this phase is usually absent in mature and well hydrated cement pastes.

CONSTRUCTION OF EMBANKMENT

The underwater embankment is almost ending up the phase 1 construction. Today, more then 70% of the embankment height is reached by staged construction. The embankment sand was put in place in layers of about 2 m, allowing a period of time in between (1 to 2 months). Currently, a longer waiting period is being allocated to allow for consolidation of the foundation soil.

The sand used for the filling operations was mainly obtained from excavation works for the construction of a dock nearby in the harbor. The sand was selected on basis of its grain size distribution and fines content. The selection of sand for the hydraulic filling operations was very important to guarantee the shear strength characteristics required for the stability of the embankment. Tests and experience showed that the execution procedure implemented here with the selected sand would yield shear angles higher than 32° ($\varphi_{cv} \cong 32°$).

As shown in figure 1, the embankment consists of a geotextile reinforced sand. Moreover, the geotextiles are anchored in geocontainers (3 m wide, 2 m high and 30 m long). The geocontainers were manufactured on land nearby the dock with a sand-cement mixture. They were transported and installed by means of a floating crane. The geotextiles were fixed to the geocontainers with steel reinforcement bars and then unrolled.

Quality control of the embankment sand was performed very regularly at all stages of the construction by means of CPT tests. Out of cone penetration tests it was possible to observe the state of the hydraulically placed sand with depth. Moreover, some correlations of shear angle (φ) and relative density were attempted. CPT tests were performed at several locations within the working area. Figures 25 and 26 do show some examples of CPT results on sand overlying the SSI improved foundation soil. The figures indicate the quality control of the embankment sand up to a level close to TAW 0.00.

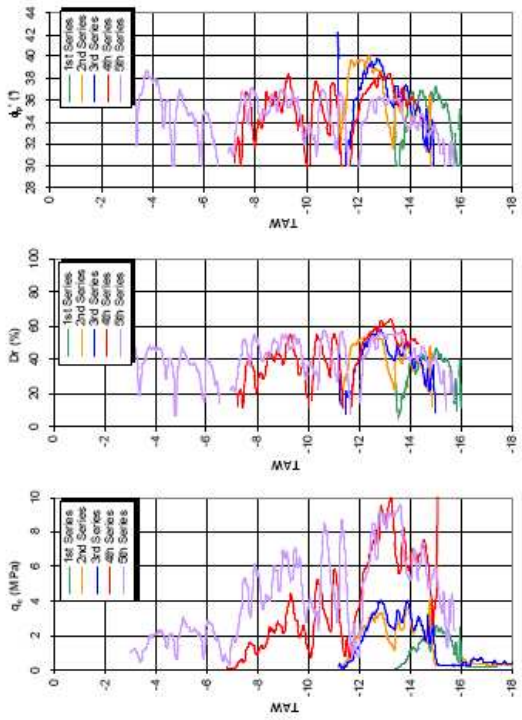

Figure 25. CPT test on sand overlying the SSI improved foundation soil, example 1

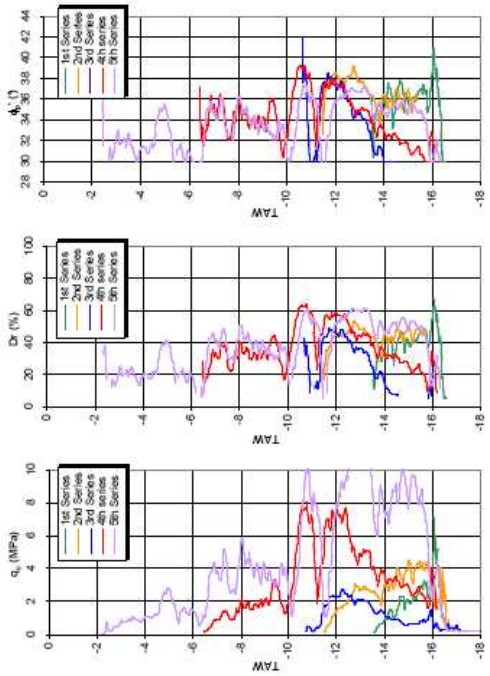

Figure 26. CPT test on sand overlying the SSI improved foundation soil, example 2.

Similarly, figures 27 and 28 show some examples of CPT results on sand overlying the non-improved (soft) foundation soil in between SSI improved soil areas. Overall, the cone penetration pressure q_c is observed to increase reaching values slightly greater than 10 MPa. However two different patterns can be identified. Sand overlying the improved zone shows low q_c values at the interface with the foundation layer (TAW -16.00) and then it increases to reach maximum values at about 3 to 4 meters above such interface (close to TAW -13.00). These patterns are probably caused due to the arching effect taking place because of the presence of SSI treated columns. The arching effect causes the sand to be most stressed some distance above the interface with foundation layer while the sand below is barely receiving any surcharge.

On the other hand, sand resistances overlying the non-improved foundation soil where there are no SSI columns do show a more regular pattern of q_c with depth. In fact, an almost linear trend was observed. The sand shear angle correlated from CPT complies, in all cases, with the design requirement of $\varphi' = 32°$.

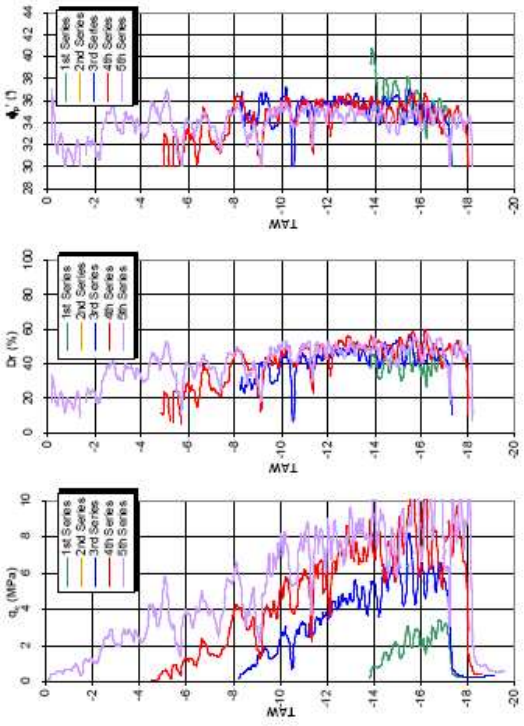

Figure 27. CPT test ons sand overlying the non-improved foundation soil, example 1

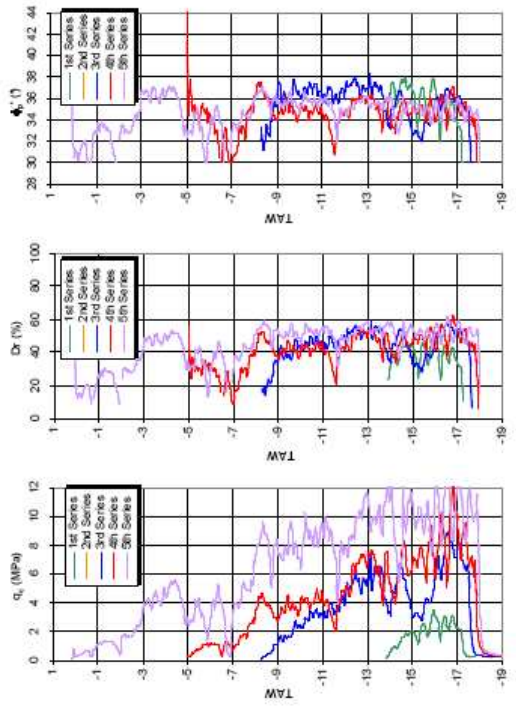

Figure 28 CPT test on sand overlying the non-improved foundation soil, example 2

Figures 29 and 30 indicate the measured settlements profiles in the non improved and the SSI improved foundation zones respectively. As expected, the largest settlements are observed in the non-improved area were up to now a maximum settlement of the order of 1.2m was measured. The maximum measured settlement in the SSI-improved zone however is of the order of 0.6m.

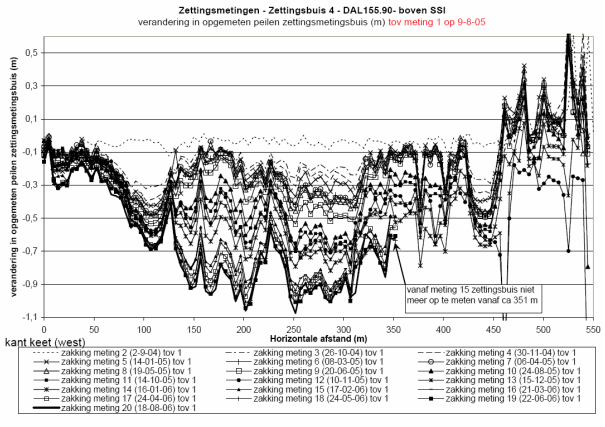

Figure 29. Settlement profile at the interface between embankment sand and foundation layer : in the SSI-treates zond

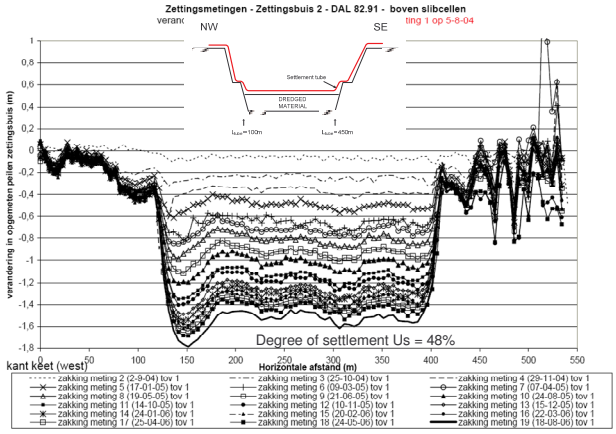

Figure 30. Settlement profile at the interface between embankment sand and foundation layer : in the non-improved zone

MONITORING OF PWP AND SETTLEMENTS

Already before the initiation of construction works, instrumentation was placed in the foundation layer to allow the monitoring of excess pore water pressures and vertical displacements under the embankment load. This continuous monitoring was meant to provide a means of following up the behavior of the foundation soil at all times during the construction.

Piezometers (P) were installed mostly at 3 different levels within the foundation layer at several locations as illustrated by the plan view sketch in figure 31.

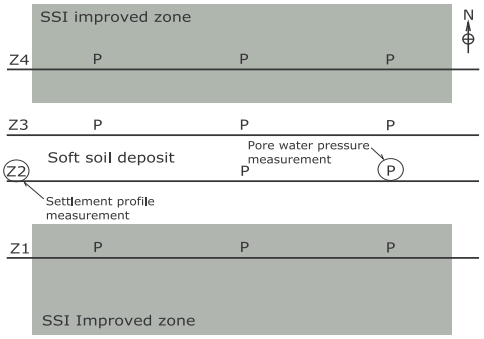

Figure 31. Scheme in plan view of instrumentation location (P : piëzometers ; Z : settlement profiles)

Piezometers in the SSI improved zones were installed between SSI columns. Similarly, flexible tubes (Z1, Z2, Z3 and Z4) filled with water were placed at 4 locations (on top of the foundation layer) across the dock to monitor vertical displacements by measuring hydraulic head changes with

respect to a reference level by means of a water pressure probe that is pulled inside the tube along its full length.

Measurements of pore water pressure have been automatically and continuously recorded, while measurements of settlement profiles were performed every 2 months approximately.

Figure 32 summarizes the measurements of excess PWP in the foundation soil during construction up to now. As expected, there is a significant difference between excess PWP measured in the soft soil deposit and those measured in the SSI improved zone (between stabilized columns). Such difference shows indeed that columns in the improved zones are carrying a significant portion of the load.

Looking at the measurements in the soft soil deposit (Fig. 32) it is possible to clearly identify the loading stages during the construction of Phase 1 that took about a year. During such period, the dissipation of PWP was not all that significant.

Later, when all construction activities in phase 1 were stopped to allow for consolidation of the foundation soil, a more pronounced dissipation was observed but still today at a low level in the order U_{pwp} = 32 % only, against a degree of consolidation as derived from the deformations of $U_{settl.}$ = 62 %.

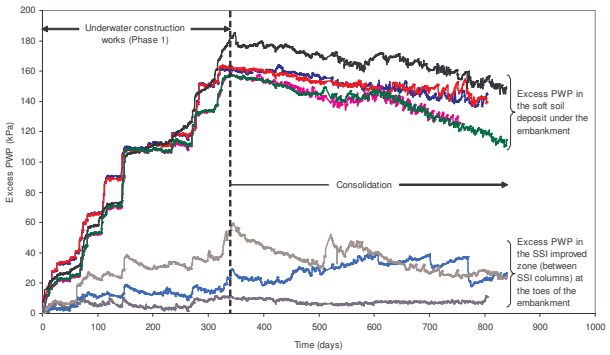

Figure 32. Excess pore water pressure measurements at various locations under the embankment

Figure 33 illustrates the settlements along the settlement tubes Z2 and Z4 (Fig. 31) on the soft soil deposit and on the SSI improved zone respectively. As expected, the largest settlements were observed in the non-improved area where up to now settlements in the order of 1.2 m to 1.3 m were measured. That is already the current load. On the other hand, the maximum measured settlements in the SSI improved zone were in the order of 0.5 m.

Out of measurements it was possible to establish that the dissipation of pore water pressures and the progress of settlements were not coupled. Less then four years after the initiation of construction works, the observed dissipation level (consolidation degree) of PWP is in the range of 32 %, while in terms of settlements 62 % of the final settlement occurred.

Such deviation of consolidation degrees evaluated out of PWP and settlement do show that the consolidation behavior of this soft foundation layer cannot be properly described by the simplified conventional consolidation theory (e.g. Terzaghi's theory).

However, when comparing the current measured consolidation degrees with those predicted introducing the large strain theory (Gibson et al., 1967), a much better match could be observed (Fig. 34).

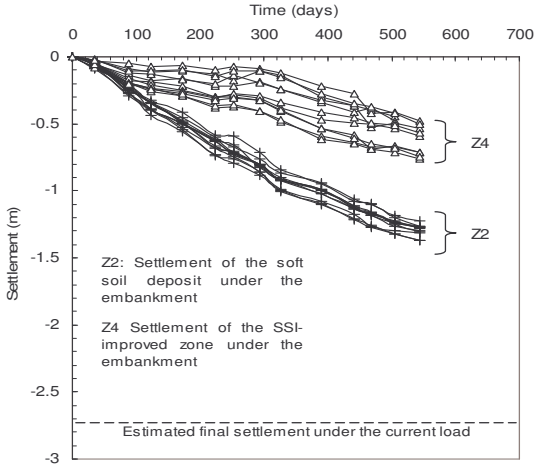

Figure 33. Settlements under the current load

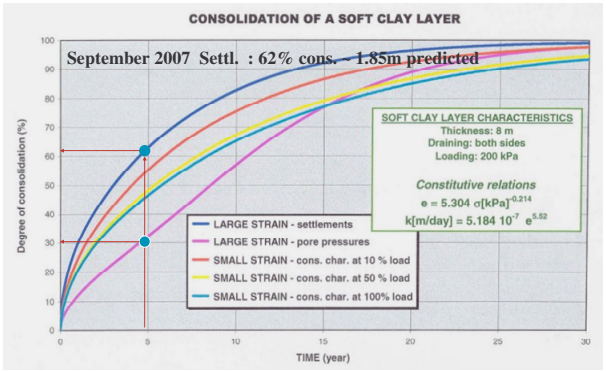

Figure 34. Large (finite) strain consolidation vs. small (inifinitesimal) strain consolidation solutions

The large strain consolidation theory is a more general theory of one-dimensional consolidation. This analysis overcomes the limitations that the conventional, small strain, theory entails; but at the same time the problem becomes so complex that only numerical solutions can be obtained for practical problems. The process of large strain) one-dimensional consolidation of a saturated porous medium is governed by:

$$\frac{\partial}{\partial z}\left[g(e)\frac{\partial e}{\partial z}\right]-b(e)\frac{\partial e}{\partial z}+\frac{\partial e}{\partial t}=0 \qquad (3)$$

where

$$g(e) = -\frac{k(e)}{\gamma_w (1+e)} \frac{d\sigma'}{de}$$

$$b(e) = \left(\frac{G_s}{\gamma_w}\right) \frac{d}{de}\left(\frac{k(e)}{1+e}\right)$$

in which e is the void ratio, γ_s and γ_w are the solid and fluid phase weights per unit of their own volume, respectively, and z is a reduced coordinate encompassing a volume of solids (Gibson et al., 1967).

The function g(e) plays the role of consolidation coefficient and b(e) introduces the effect of gravity. If the gravity effect is neglected [i.e. b(e) = 0] and g(e) is assumed to remain constant during the process, then equation 3 simplifies into the classical theory (i.e. Terzaghi's). Equation 3, can be numerically solved with appropriate boundary and initial conditions and making use of the constitutive equations (Eq. 1&2) of the soft soil.

To that end a finite difference based program (Van Impe P.O., 1999) was used to perform calculations. Results of large strain consolidation and small strain consolidation evaluation are compared in figure 34.

In this simulation, a single load increment (equal to the current load) was applied to the homogeneous 8 m thick soft soil layer. Moreover, the output of small strain analysis is showed as a range because there is a range of consolidation coefficients that can be chosen out of the constitutive equations of the soft soil for the full range of stress levels it will be subjected to.

The outcome of the monitoring of the consolidation behavior of the soft soil matches closely the estimations evaluated using the large strain consolidation theory. In fact, figure 34 shows that the estimated consolidation degree out of settlements after 3.5 years of loading.

Moreover, it can be concluded that small strain consolidation predictions could give unsafe results when designing a staged construction on soft soil since it overestimates the consolidation degree out of pore water pressures which could lead to overestimation of strength gain due to consolidation.

QUALITY CONTROL OF THE HYDRAULIC FILL

Quality control of the embankment sand was performed regularly at several stages during the construction by means of CPT tests. Moreover, parameters such as shear angle (φ) and relative density could be estimated to confirm the design requirements. An example of typical CPT profile above the soft soil deposit is given in figure 35. It can be observed that the cone pressure q_c increases linearly with depth and an almost uniform shear angle ranging from 32° to 35° was evaluated.

Furthermore, the risk of liquefaction of this hydraulic fill was assessed using the method proposed by Robertson and Wride (1998). For characterizing the local seismicity in the area, an earthquake magnitude of M=5.5 was assumed and a Peak Ground Acceleration (PGA) of 0.05g was obtained from the seismic zonation map of Belgium. Making use of those data a factor of (FoS) was evaluated (Fig. 35). In all cases FoS against liquefaction did exceed 1, in fact most factors ranged from FoS = 2.5 to 6. It can be concluded that liquefaction, for an earthquake magnitude of 5.5, will not occur.

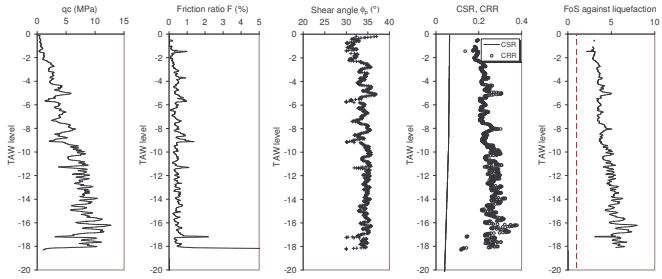

Figure 35. Some properties of the hydraulically placed embankment sand

CONCLUSIONS

The monitoring of the consolidation behavior of a soft foundation soil under a large partially submerged sand embankment has shown that the large strain consolidation theory was successful to describe more adequately such behavior. Measurements of settlements and excess pore water pressures showed a good agreement with predictions evaluated using the large strain consolidation theory. On the other hand, the more conventional small strain theory was shown to overestimate the dissipation of pore water pressure and underestimate settlements. This could lead to an unsafe design of staged construction. The state-of-the-art report on the use of underwater geosynthetics has been discussed under item 7.

Geosynthetics are of major importance in different hydraulic engineering applications. Different types of geosynthetics are maintaining interdisciplinary functions of filtration, drainage, separation, reinforcement, erosion protection and sealing-/lining. As new generation of filter geotextiles sand mats are specially developed for hydraulic engineering applications, where an underwater installation of filtration geotextiles under currents is required. Encapsulating soil (mainly sand) into geotextile containers or tubes provide construction elements for a variety of economical and ecological applications e.g. for dams, dikes, erosion control, scour protection, breakwaters, groynes and dune protection.

REFERENCES

Bräu, G., Floss, R. 2000. Geotextile structures used for the reconstruction of the motorway Munich-Salzburg. Proceedings of the Second European Geosynthetics Conference, EuroGeo 2000, Bologna, pp 373 – 377.

Bussert, F. 2006. Verformungsverhalten geokunststoffbewehrter Erdstützkörper - Einflussgrößen zur Ermittlung der Gebrauchstauglichkeit. Schriftenreihe des Instituts für Geotechnik und Markscheidewesen der TU Clausthal. Heft 13/2006.

EBGEO 1997. Empfehlungen für Bewehrungen aus Geokunststoffen. Deutsche Gesellschaft für Geotechnik e.V. (DGGT), Ernst & Sohn publishing company, Berlin, Germany.

Edwards, R., Smith, S. 2003. Optimising biodiversity of macroin-vertebrates on artificial reefs. AMSA National Conference, Australia.

Gibson et al. 1967. The theory of 1D consolidation of saturated clay: finite non-linear consolidation of thin homogeneous layers. Geotechnique, Vol. 17, No. 3, pp. 261-273.

Heerten, G. 1980. Long-term experiences with the use of synthetic filter fabrics in coastal engineering. Proceedings 17th ICCE, Australia.

Heerten, G., Jackson, A., Restall, S., Saathoff, F. 2000. New Developments With Mega Sand Containers of Nonwoven Needle-Punched Geotextiles for the Construction of Coastal Structures. ICCE, Australia.

Heerten, G., Werth, K. 2005. Geosynthetics in the marine environment. Baltic Geotechnics X on Geotechnical Engineering for Harbours, Onshore and Near Shore Structures, 12-14 October 2005, Riga, Latvia.

Heerten, G., Lenze, B., Pries, J. K. 2005. Geosynthetics in the Marine Environment. 1st Portugese Seminar on Geosynthetics, Porto, Portugal, November 2005.

Herle, V. 2006. Long-term performance of reinforced soil structures, Active geotechnical design in infrastructure development. Proceedings of the 13th Danube-Conference on Geotechnical Engineering, Slovenian Geotechnical Society, Ljubljana, Slovenia, 2: 251-256.

Nickels, H., Heerten, G. 2000. Objektschutz Haus Kliffende. HANSA – Schiffahrt – Schiffbau – Hafen – 137. Jahrgang – 2000 – Nr. 3, pp. 72 – 75.

Pachomow, D., Vollmert, L., Herold, A. 2007. Der Ansatz des horizontalen Erddruckes auf die Front von KBE-Systemen. 10. Informations- und Vortragstagung über Kunststoffe in der Geotechnik, FS-KGEO 2007, München, Februar 2007.

Restall, S. Jackson, A., Heerten, G., Hornsey, W. 2002. Case studies showing the growth and development of geotextile sand containers: an Australian perspective. Geotextiles and Geomembranes 20, pp 321 – 342.

Restall, S., Hornsey, W., Oumeraci, H., Hinz, M., Saathoff, F., Werth, K. 2004. Australian & German experiences with geotextile containers for coastal protection. EUROGEO 3, Germany

Robertson P.K., & Wride C.E. 1998. Evaluating cyclic liquefaction potential using the cone penetration test. Canadian Geotechnical Journal, Vol. 35. pp.: 442–459.

Tatsuoka, F., Tateyama, M., Uchimura, T., Koseki, J., 1996. Geosynthetic-Reinforced Soil retaining Walls as Important permanent Structures. Geosynthetics International 1997, Volume 4, No. 2.

Turner, L. 2003. Applications of coastal imaging technology to Coastal Engineering and Coastal Management in Australia. Coasts & Ports, New Zealand.

Van Impe W.F., Verastegui Flores R.D. 2006. Deep mixing in underwater conditions: a laboratory and field study. Ground Improvement , Vol. 10, No. 1, pp. 15-22.

Van Impe W.F., Verastegui Flores R.D, Underwater embankments on soft soil : a case history, Taylor and Francis , London UK (2007).

Van Impe P.O. 1999. Consolidation of saturated, highly compressible porous media. MsC thesis, Faculty of engineering, UGent (in dutch).

Ziegler, M., Heerten, G., Retzlaff, J. 2007. A new dimensioning approach for junction stiff geogrids. XIV European Conference on Soil Mechanics and Geotechnical Engineering, Madrid, Spain, September 2007.